Protein Cell 2010, 1(5): 491–500
DOI 10.1007/s13238-010-0061-7

Protein & Cell

RESEARCH ARTICLE

Structures of EV71 RNA-dependent RNA polymerase in complex with substrate and analogue provide a drug target against the hand-foot-and-mouth disease pandemic in China

Yang Wu[1*], Zhiyong Lou[2*], Yi Miao[2], Yue Yu[2], Hui Dong[2], Wei Peng[1], Mark Bartlam[3], Xuemei Li[1], Zihe Rao[1,2,3] ✉

[1] National Laboratory of Macromolecules, Institute of Biophysics, Chinese Academy of Sciences, Beijing 100101, China
[2] Structural Biology Laboratory, Tsinghua University, Beijing 100084, China
[3] College of Life Sciences and Tianjin State Laboratory of Protein Science, Nankai University, Tianjin 300071, China
✉ Correspondence: raozh@xtal.tsinghua.edu.cn
Received April 18, 2010 Accepted April 30, 2010

ABSTRACT

Enterovirus 71 (EV71), one of the major causative agents for hand-foot-and-mouth disease (HFMD), has caused more than 100 deaths among Chinese children since March 2008. The EV71 genome encodes an RNA-dependent RNA polymerase (RdRp), denoted $3D^{pol}$, which is central for viral genome replication and is a key target for the discovery of specific antiviral therapeutics. Here we report the crystal structures of EV71 RdRp ($3D^{pol}$) and in complex with substrate guanosine-5'-triphosphate and analog 5-bromouridine-5'-triphosphate best to 2.4 Å resolution. The structure of EV71 RdRp ($3D^{pol}$) has a wider open thumb domain compared with the most closely related crystal structure of poliovirus RdRp. And the EV71 RdRp ($3D^{pol}$) complex with GTP or Br-UTP bounded shows two distinct movements of the polymerase by substrate or analogue binding. The model of the complex with the template:primer derived by superimposition with foot-and-mouth disease virus (FMDV) 3D/RNA complex reveals the likely recognition and binding of template:primer RNA by the polymerase. These results together provide a molecular basis for EV71 RNA replication and reveal a potential target for anti-EV71 drug discovery.

KEYWORDS enterovirus 71, RNA-dependent RNA polymerase, crystal structure, drug target

INTRODUCTION

Between March and June 2008, an outbreak of hand-foot-and-mouth disease (HFMD) occurred in China. More than 9 provinces were affected, including Beijing and Shanghai, with Anhui and Guangdong provinces in East and Southern China, respectively, among the most seriously affected. During the course of the outbreak, more than 176,000 cases of infection were reported and at least 100 individuals died (Yang et al., 2009). HFMD has also been reported in Australia, the Asia-Pacific region, and several European countries since its appearance (McMinn, 2002). During recent years, HFMD surveillance has shown increasing infections in the Asia-Pacific region, especially in Malaysia, Singapore, Taiwan and mainland China. Since its discovery in 1969, Enterovirus 71 (EV71) has been recognized as a frequent cause of HFMD epidemics associated with a severe form of brainstem encephalitis, as well as with pulmonary edema, and it therefore causes high fatality rates (Yang et al., 2009).

EV71, which belongs to the human Enterovirus A species of the *Enterovirus* genus within the family *Picornaviridae* (King, 2000), has a single-stranded, positive-sense RNA

[*] These authors contribute equally to this work

genome of approximately 7.5 kb. The EV71 genome encodes a ~250 kDa polyprotein (P3), which is cleaved by the viral protease into several proteins required for viral reproduction. An RNA-dependant-RNA-polymerase (RdRp), also known as $3D^{pol}$, is located in the most down-stream part of the cleaved polyprotein (Fig. 1A) and is responsible for replicating the initial negative-strand and the subsequent infecting positive-strand RNA (Racaniello, 2001).

To date, representative RdRps from five families of RNA viruses have known three-dimensional structures: (1) *Picornaviridae*, poliovirus (Hansen et al., 1997; Thompson and Peersen, 2004; Thompson et al., 2007), human rhinovirus (Love et al., 2004), coxsackievirus (Campagnola et al., 2008), foot-and-mouth-disease virus (FMDV) (Ferrer-Orta et al., 2004); (2) *Caliciviridae*, rabbit hemorrhagic disease virus (Ng et al., 2002), Norwalk virus (Zamyatkin et al., 2008); (3) *Flaviviridae*, hepatitis C virus (Bressanelli et al., 1999; Lesburg et al., 1999), bovine viral diarrhea virus (Choi et al., 2006), Dengue virus (Yap et al., 2007), West Nile virus (Malet et al., 2007); (4) *Cystoviridae*: phage ϕ6 (Butcher et al., 2001; Salgado et al., 2004); and (5) *Reoviridae*, reovirus (Tao et al., 2002). The RdRp enzymes share a similar overall structure

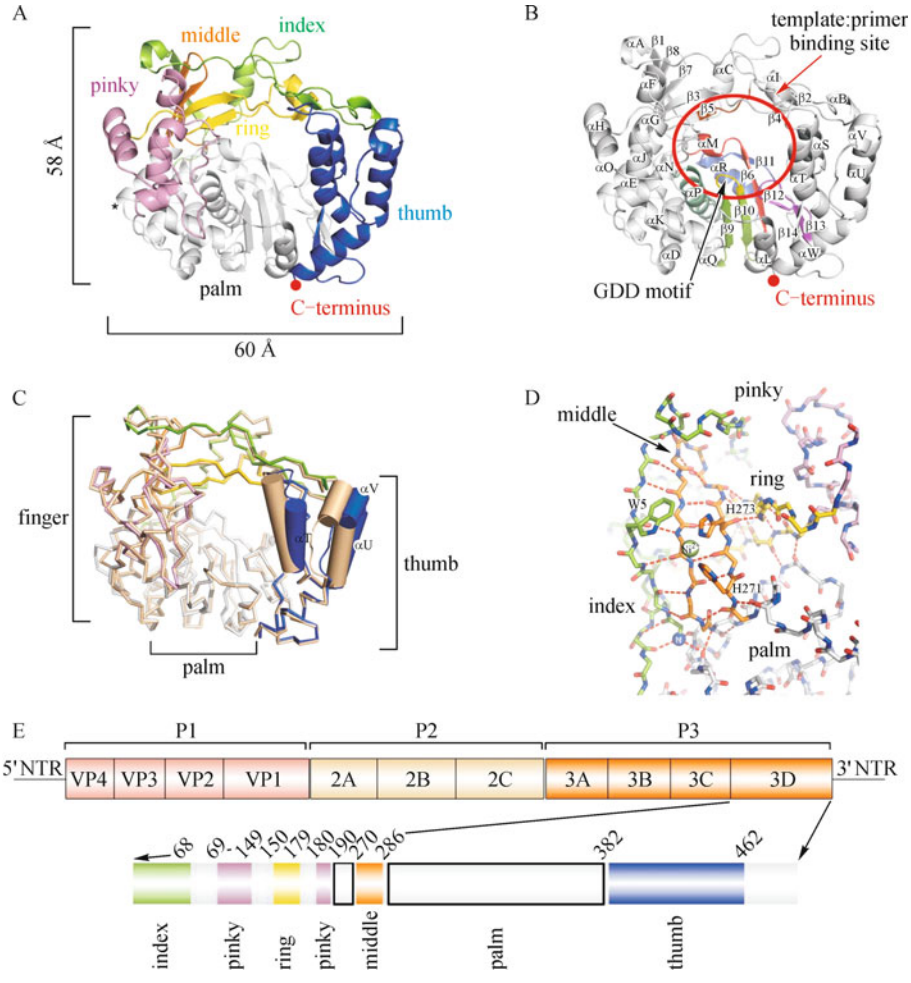

Figure 1. Overview of the EV71 RdRp ($3D^{pol}$) structure. (A) The EV71 RdRp ($3D^{pol}$) structure is colored according to the convention previously used for poliovirus $3D^{pol}$ (Thompson and Peersen, 2004); index finger (residues 1–68) in green, ring finger (150–179) in yellow, pinky finger (96–149,180–190) in pink, middle finger (270–286) in orange, palm (191–269, 287–381) in gray, thumb (382–462) in blue. The extra residue Glu260 in EV71 RdRp is marked with an asterisk. (B) Conserved polymerase motifs of the EV71 RdRp ($3D^{pol}$) are as follows: motif A (red; 229–241), motif B (cyan; 293–310), motif C (green; 321–336), motif D (blue; 340–357), motif E (magenta; 370–380), motif F (brown; 172–176) and the GDD sequence in motif C (yellow; 328–320). (C) Structures of EV71 (multicolored as in A) and poliovirus (PDB 1RA6, wheat) polymerases superimposed using Pymol alignment of all residues, exhibiting the movement of the thumb domains. (D) The extensive network of hydrogen bonds linking the N-terminus (blue sphere at lower left), the index (green), middle (orange) and ring (yellow) fingers and palm (pale) domain altogether. The Ni^{2+} ion (lime sphere) is coordinated by the side chains of His271, His273 and Cys282 in the middle finger, strengthening the interaction network. The view is 180° relative to Fig. 1A. (E) Genome organization of EV71. The single ORF is flanked by UTRs at the 5' and 3' ends. $3D^{pol}$ is positioned in the P3 region and is colored according to the structural elements shown in Fig. 1A.

with “fingers”, “palm”, and “thumb” domains arranged in a cupped, “right hand” configuration. In addition to the three basic domains, an N-terminal domain bridging the fingers and thumb domains is found in all RdRps (Ng et al., 2008). The distantly related DNA-dependent DNA polymerases (DdDps), DNA-dependent RNA polymerases (DdRps), and RNA-dependent DNA polymerases (RdDps or reverse transcriptases) all share the same basic architecture with the RdRps. Although polymerases from different classes share only low levels of amino acid sequence identity, the observation of conserved structural elements in evolutionarily distant species suggests they serve important functional roles.

The picornaviral polymerases are unique in that they only become active upon complete proteolytic processing of the precursor $3CD^{pro}$ (Andino et al., 1993; Thompson and Peersen, 2004; Marcotte et al., 2007). The structure of the poliovirus RdRp revealed that the N-terminal glycine residue of the fully processed polymerase is buried in a pocket at the base of the “fingers” domain, where it involves in four hydrogen bonds that effectively reposition Asp238 into the active site. Asp238 is then able to form a 2.8-Å long hydrogen bond interaction with the 2' hydroxyl of the incoming ribonucleoside triphosphates (NTPs), while it extends away from the protein as part of a flexible interdomain linker in the structure of the $3CD^{pro}$ (Thompson and Peersen, 2004; Campagnola et al., 2008).

Because of its population that circulated as a mutant swarm or viral quasispecies, there still are no vaccines or therapeutics known to be effective in preventing or treating EV71 infection (Domingo et al., 2008). Effective therapeutics are urgently needed to treat the pandemic of HFMD in China and worldwide. Since the viral RdRp plays a central role in the life cycle of RNA viruses, and specific inhibitors of the RdRp should therefore serve as potential anti-viral agents.

RESULTS AND DISCUSSION

Molecular folding of EV71 RdRp ($3D^{pol}$)

The crystal structure of EV71 RdRp ($3D^{pol}$) was determined to 2.6 Å resolution with a final R_{work} value of 21.9% (R_{free} = 26.9%) by molecular replacement with the crystal structure of the poliovirus polymerase, sharing 67.1% sequence identity (PDB code: 1RA6) (Thompson and Peersen, 2004), as an initial search model. The crystal of EV71 RdRp ($3D^{pol}$) belongs to the space group $P3_221$ with the cell parameters of $a = b = 103.5$ Å, $c = 132.4$ Å. We assumed the presence of one monomer per asymmetric unit with a Matthews coefficient of 3.84 $Å^3$/Da, corresponding to a solvent content of 67.7% (Matthews, 1968). The crystal structure of EV71 RdRp ($3D^{pol}$) in complex with GTP and Br-UTP were determined to 2.4 Å and 2.9 Å, respectively. The overall refined structures, which share the same overall architecture with native EV71 RdRP ($3D^{pol}$), show two distinct differences around the rNTP binding site corresponding to substrate and analogue binding, and were of good quality with reasonable stereochemistry. Final statistics are summarized in Table 1.

The overall crystal structure of EV71 RdRp ($3D^{pol}$) adopts the usual closed “right-hand" conformation observed for other RdRps, which is composed of “fingers”, “palm” and “thumb” domains (Fig. 1A) (Ferrer-Orta et al., 2006) with approximate dimensions 63 Å × 51 Å × 61 Å, which is formed by 23 α-helices (αA–αW) and 14 β-strands (β1–β14) (Fig. 1B). The EV71 RdRp ($3D^{pol}$) generally shares structure/sequence similarity with homologous RdRps from poliovirus (Thompson and Peersen, 2004), coxsackievirus (Campagnola et al., 2008) rhinovirus (Love et al., 2004) and FMDV (Ferrer-Orta et al., 2004) polymerases in *Picornaviridae* family. The EV71 RdRp ($3D^{pol}$) has six four-amino-acid sequence conserved motifs, which are termed motif A, B, C, D, E and F respectively. Motif A, B, C and D, located in the palm domain, are defined in all classes of polymerases, whereas motif E in the palm domain and motif F in the fingers domain are unique to both RdRps and reverse transcriptases (RTs) (Fig. 1B) (Poch et al., 1989; Hansen et al., 1997; O'Reilly and Kao, 1998). The fingers domain can be further subdivided into five distinct finger motifs, which are named as index, pinky, middle and ring fingers as indicated in the homologous structures in the *Picornaviridae* family (Ferrer-Orta et al., 2006). The index finger protrudes into the thumb domain via insertion of Phe30 and Phe34 into the hydrophobic core at the top of the thumb and encircles the active site of the enzyme. This enclosed conformation forms a large cavity 18 Å across and 22 Å deep at the center of the molecule for template:primer RNA binding in the front of the polymerase, and creates a small positively charged channel 8 Å across and 14 Å deep on the back side for the recruitment of NTPs into the active site for further RNA replication. Compared with the sequence of the poliovirus polymerase which is most closely related to phylogenetically among structure-determined RdRps, the EV71 RdRp ($3D^{pol}$) contains an extra residue, Glu260, at the N-terminal of the helix αO (residues Glu260–Asn270), surface exposed (Fig. 1A). Interestingly, the trend is also observed in coxsackievirus RdRp (Campagnola et al., 2008). The superimposition by Pymol alignment of all residues suggests that the thumb domain of EV71 RdRp ($3D^{pol}$) opens approximately 12° wider than in poliovirus polymerase (Fig. 1C). The main reason for the movement we propose here is that Ala408 in EV71 RdRp ($3D^{pol}$) substitutes for corresponding proline at the N-terminal of the helix αT in poliovirus polymerase (Fig. 1C). The substitution breaks the N-terminal of αT, making it shorter and loosing the thumb domain outward.

In the crystal structure of the EV71 RdRp ($3D^{pol}$), strong electron density is observed adjacent to the side chains of His271, His273 and Cys282 in the middle finger, and is occupied by a divalent nickel ion derived from the crystallization conditions as a crucial additive reagent for EV71 RdRp ($3D^{pol}$) crystallization. The Ni^{2+} coordinates with the

Table 1 Data collection and refinement statistics

parameters	EV71 $3D^{pol}$	$3D^{pol}$/GTP	$3D^{pol}$/Br-UTP
data collection			
space group	$P3_221$	$P3_221$	$P3_221$
cell parameters (Å, °)	$a = b = 103.5$, $c = 132.4$ $\alpha = \beta = 90°$, $\gamma = 120°$	$a = b = 103.5$, $c = 133.0$ $\alpha = \beta = 90°$, $\gamma = 120°$	$a = b = 103.5$, $c = 131.5$ $\alpha = \beta = 90°$,$\gamma = 120°$
wavelength (Å)	1.0000	1.0000	1.0000
resolution range (Å)[a]	89.4−2.6 (2.64−2.60)	50.0−2.4 (2.49−2.40)	50.0−2.9 (29.6−29.0)
R_{merge} (%)[b]	6.5 (40.8)	9.5 (67.2)	7.1 (92.5)
No. of all observed reflections	370,541 (13,716)	623,499 (25,607)	382,586 (10,691)
No. of unique reflections	25,646 (1256)	32,854 (3129)	18,561 (1028)
completeness (%)	99.8 (99.1)	100.0 (99.9)	99.9 (99.4)
I/σ (I)	51.2 (4.1)	12.3 (1.3)	53.4 (2.0)
structure refinement			
resolution range (Å)	89.4−2.6	89.8−2.5	89.8−2.9
No. of reflections used	24,319	27,582	17,611
R_{work} (%)	21.9	19.4	23.3
R_{free} (%)[c]	26.9	24.9	27.3
No. of protein atoms	3700	3700	3700
No. of solvent/metal atoms	97	231	19
overall average B-factor (Å^2)	49.1	43.9	96.1
r.m.s. deviation			
rmsd bond lengths (Å)	0.017	0.013	0.006
rmsd bond angles (°)	1.757	1.514	1.001

[a] Values in parentheses refer to the highest resolution shell.

[b] $R_{merge} = \Sigma_h\Sigma_i \mid I_{ih} - < I_h > \mid / \Sigma_h\Sigma_i < I_h >$, where $< I_h >$ is the mean of multiple observations I_{ih} of a given reflection h.

[c] $R_{work} = \Sigma||F_p(obs)|-|F_p(calc)||/ \Sigma|F_p(obs)|$; R_{free} is an R-factor for a selected subset (5%) of reflections that was not included in prior refinement calculations.

side chains of His271, His273 and Cys282 strengthening the hydrogen bonds interaction network (Thompson and Peersen, 2004) (Fig.1D). And this surface metal binding of EV71 RdRp ($3D^{pol}$) may be unique among the picornaviruses, for His271, His273 and Cys282 are not conserved (Fig. 2).

The interaction between EV71 RdRp ($3D^{pol}$) and bounded GTP/ Br-UTP

X-ray diffraction analysis of EV71 RdRp ($3D^{pol}$) crystals soaked with GTP and 5-bromouridine 5'-triphosphate (Br-UTP) under the conditions described in Materials and Methods revealed extra density around the ribonucleotide (rNTP) binding site of the EV71 RdRp ($3D^{pol}$), suggesting the affinity of the $3D^{pol}$ for nucleotide and nucleotide analogs is therefore sufficiently high to provide unambiguous electron density. The bound GTP molecule was built into the rNTP binding site near the catalytic center of the $3D^{pol}$ under the guidance of unambiguous electron density map, bound in the syn conformation with the base swung over the ribose, which is similar to the conformation observed in its homologues, poliovirus and FMDV RdRps ($3D^{pol}$) (Thompson et al., 2007; Ferrer-Orta et al., 2009) (Fig. 3A). Compared with the native EV71 RdRp ($3D^{pol}$), there are two obvious conformational changes in $3D^{pol}$/GTP complex as a result of GTP binding (Fig. 3C). The loop region, L1, which consists of Ser289-Gly293 and the N-terminal of motif B, flips towards the base moiety of GTP by 60° at maximum. Although conformational changes of the similar region, the loop called β9-α11, on different NTP binding were previously described in the structures of FMDV 3D elongation complexes (Ferrer-Orta et al., 2009), the rearrangement of L1 we reported here is much more distinct by GTP binding. Ser289 in L1, which is highly conserved in picornaviral RdRps (Fig. 2), moves the farthest, 5.7 Å, participating in the interaction network of GTP binding. Moreover, the trace of region Thr356–Asn368, L2, in the large loop between motif D and motif E rearranges a little to fit the bound GTP molecule. The surrounding residues

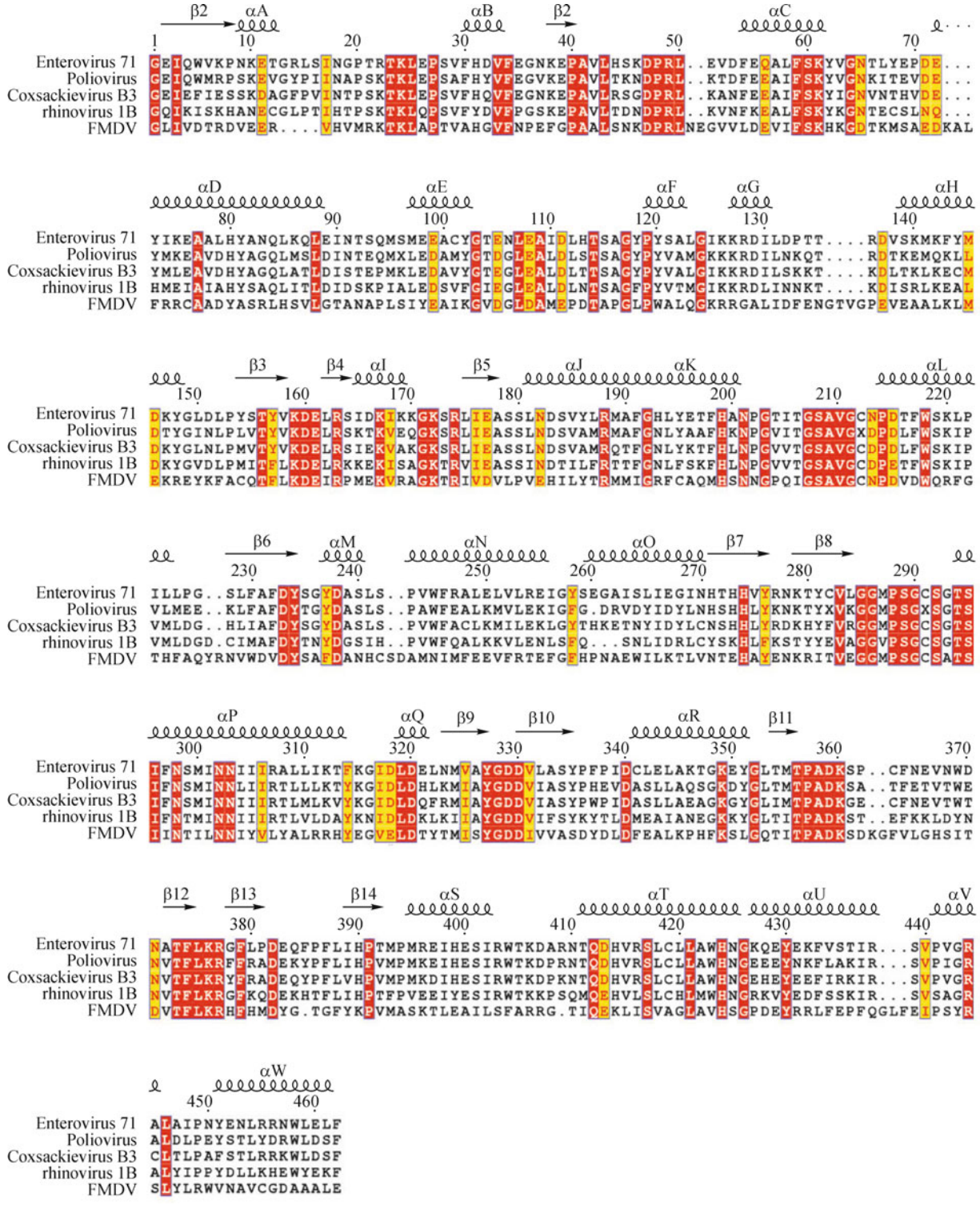

Figure 2. Sequence alignment of the RNA dependent RNA polymerase from EV71, poliovirus, coxsackievirus B3, rhinovirus 1B and FMDV. Secondary structure elements of EV71 RdRp ($3D^{pol}$) are marked on top of the alignment; α-helices and β-strands are presented as curves and arrows, respectively. The number of residues on the top refers to EV71 RdRp ($3D^{pol}$) sequence.

envelop the GTP, forming an extensive hydrogen-bonded network and electrostatic interactions, which are responsible for binding and positioning the GTP (Fig. 3B). Asp238 is vital for the polymerase fidelity by sensing the 2' hydroxy group of GTP. Its side-chain is thus bridged by Asn298 and the flipped Ser289 on two sides forming 3.17 Å and 2.49 Å hydrogen bonds, and hydrogen bonded with the 2' hydroxy group of GTP with a distance of 2.78 Å. Arg174, in motif F, forms a hydrogen bond with the ribose ring oxygen. The guanidinium group of Arg174, locked by a charge interaction with Glu161, makes a cation-π stacking interaction with the base moiety of GTP. On the other side of the moiety group, the flipped Ser289 forms hydrogen bonds with Asp238 and the backbone of Glu177. Moreover, the backbone of Leu175 contacts with the base moiety by hydrogen bonds with the N1 and N2 atoms at respective distances of 2.77 Å and 3.02 Å. Furthermore, the triphosphate moiety is involved in the positively charged environment of NTP entry tunnel. It makes ionic interactions with Lys167 and Arg163 of the ring finger. Additionally, β- and γ-phosphate form hydrogen bonds with Gly236 and Ser235 at distances of 2.56 Å and 3.12 Å, respectively.

To elucidate the potential mechanism for inhibitor design to target EV71 RdRp ($3D^{pol}$), several ribonucleotide analogs were investigated by crystallographic and biochemical methods. The $3D^{pol}$ complexed with substrate analog Br-UTP shares general similarity with the $3D^{pol}$/GTP complex (Fig. 3C), although the electron density for Br-UTP is not as well defined as that for GTP, suggesting a relatively lower binding affinity and higher B-factors. Br-UTP, in the NTP binding site, is in the lower-energy anti conformation with the base swung away from the sugar. The 3'-OH group of the sugar moiety forms a hydrogen bond with the side chain of Asp238 at a distance of 2.98 Å. However, the base does not form any hydrogen bonds with the enzyme. Moreover, the bromide atom on the base moiety protrudes to the carbonyl atom of Leu175, whereas the loop L1 flips a little less than by GTP binding, and Ser289 forms a hydrogen bond only with the backbone of Leu175 instead of interacting with the side chain of Asp238 in the crystal structure of $3D^{pol}$/GTP. All of

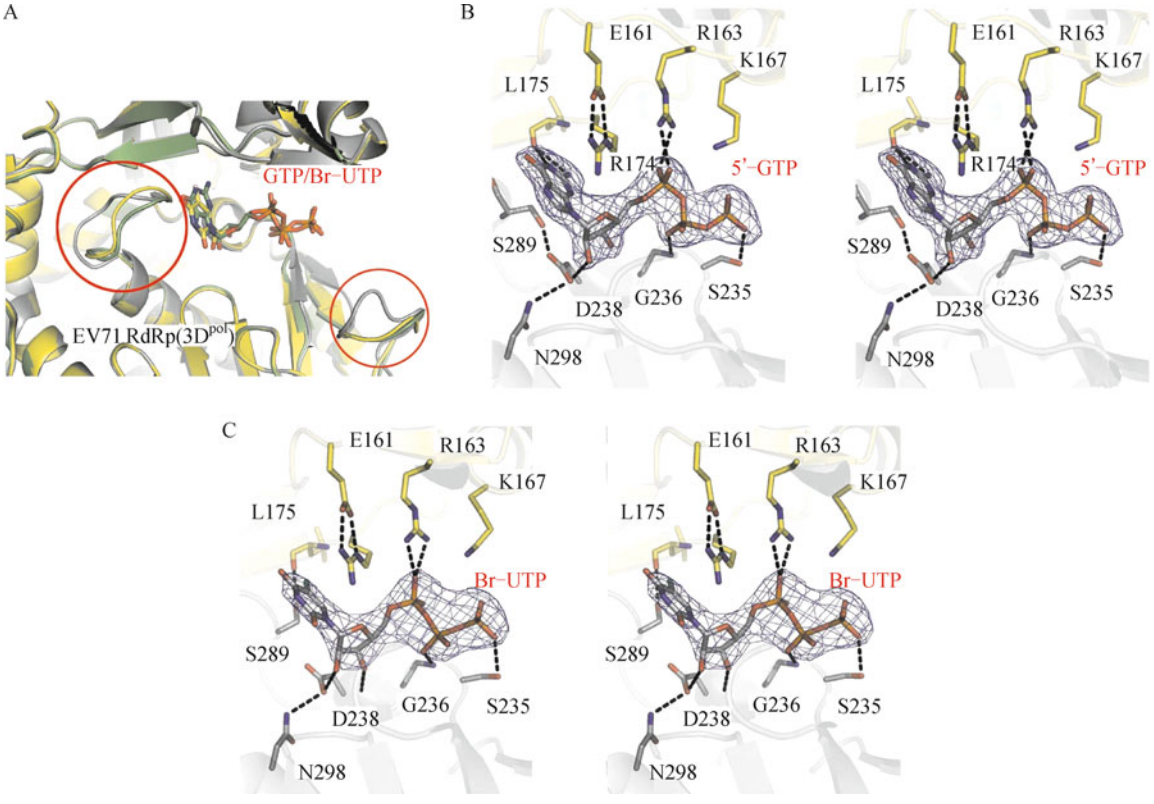

Figure 3. Structure of EV71 RdRp ($3D^{pol}$) complexed with GTP or Br-UTP. (A) Superimposition of the structures of EV71 RdRp $3D^{pol}$/ GTP (green) and $3D^{pol}$/Br-UTP (yellow) with the native EV71 RdRp ($3D^{pol}$) (pale) showing the two main changes upon ligand binding. (B) Stereo diagram of NTP binding site in EV71 RdRp $3D^{pol}$/GTP. Electron density of SA-omit map corresponding to the GTP is shown in blue mesh at a contour level of 1.0 σ. Hydrogen bonds are represented by black dotted lines. View is taken in the front of the polymerase. (C) Stereo diagram of NTP binding site in EV71 RdRp $3D^{pol}$/Br-UTP. Electron density of SA-omit map corresponding to the Br-UTP is shown in blue mesh at a contour level of 1.0 σ. Hydrogen bonds are represented by black dotted lines. The view shows the front of the polymerase.

these factors ensure that the interaction of the ribonucleotide analogue Br-UTP in the NTP binding site is less strong than the interaction of the native substrate GTP. However, the conformational changes in EV71 RdRp (3D^{pol}) after Br-UTP bounded obtain the very similar tendency with those by GTP (Fig. 3C), which supports the hypothesis that specific movements of EV71 RdRp (3D^{pol}) are trigged by substrate binding and provides unique crystal structure information shedding light on EV71 RdRp (3D^{pol}) inhibitor design. Furthermore, the location of triphosphate group is almost the same among the complex crystal structures of picornaviral RdRps, and has the strongest electronic density in ribonucleotide binding region, which suggests a significant reach for the inhibitor development. Additionally, no distinct interactions were observed from Biacore results even at GTP and Br-UTP concentrations of 5 mM, so equilibrium presumably exists between EV71 RdRp (3D^{pol}) and its substrates.

Model of EV71 RdRp (3D^{pol}) complex with template:primer

In order to better understand template:primer recognition and binding by EV71 RdRp (3D^{pol}), we could model its complex with the template:primer based on the crystal structure of EV71 RdRp (3D^{pol}) and reported homologues. Two features enable us to build a feasible model using the EV71 RdRp apoenzyme structure: the direction of polymerase translocation along the template strand is consistent among the known polymerase structures; and the nascent nucleic acid duplex is known to adopt an approximate A-form conformation in the immediate vicinity of the active site (Jacobo-Molina et al., 1993; Doublie et al., 1998; Huang et al., 1998; Li et al., 1998; Lesburg et al., 1999). We therefore modeled the structure of EV71 RdRp (3D^{pol}) in complex with the template:primer (5'-CAUGGGCC-3'/5'-GGCCC-3') by superimposing the palm domain with the structure of the FMDV 3D polymerase in complex with the template:primer RNA (PDB code: 1WNE) (Ferrer-Orta et al., 2004) (Fig. 4).

Regions of the index finger (Ser16–Thr21), ring finger (Ser155–Glu158, Arg174–Ala178) and little finger (His113–Leu130) create the entrance of a well-defined channel which is suitably large enough to facilitate single strand template RNA binding, and which extends towards the large exposed active site. The large, positively charged area of the index finger at the top of the entrance may help to stabilize the template RNA and break its secondary structure. The template:primer RNA, forming a right-handed A-form helix with Watson-Crick base pairing, fits well into the large cavity in the front of EV71 RdRp (3D^{pol}). The template strand mainly forms contacts with residues in the fingers domain, whereas the primer strand interacts largely with the thumb domain. The third nucleoside of the template is located at the P site with its base facing the active center of the phosphoryl transfer reaction predicted from the FMDV 3D/RNA crystal

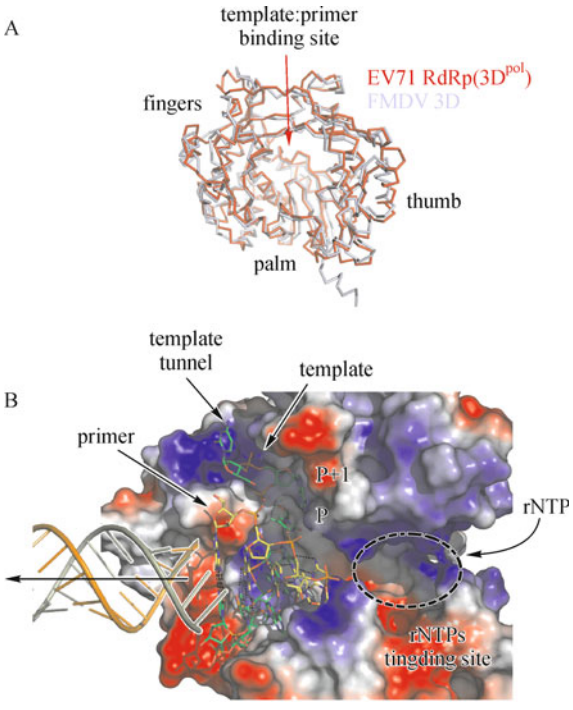

Figure 4. Structural model of EV71 RdRp (3D^{pol}) complexed with template:primer RNA. (A) Superimposition of the structures of EV71 (red) and FMDV (light blue) polymerases using Pymol alignment of all residues, showing no significant difference between the two polymerases. (B) Electrostatic potential surface representation of EV71 RdRp (3D^{pol}) showing a large, exposed central cavity in which the template:primer RNA can be accommodated. The view shows the front of the polymerase with thumb (382–462) and index (25–41) domains deleted. Positive and negative charges are indicated in blue and red, respectively.

structure. The incoming NTP, matching Watson-Crick base pairing, would contact with Mg^{2+} coordinated on the GDD motif and trigger the phosphoryl transfer reaction.

CONCLUSIONS

The EV71 RNA-dependent RNA polymerase (3D^{pol}) is critical in the viral life-cycle, and is considered to be a potential target for drug discovery based on its importance to the virus, its structure/sequence conservation and its low homology with human proteins. We determined the crystal structure of the full-length EV71 RdRp (3D^{pol}), which adopts the typical "closed-right-hand" conformation of RdRp structures complete with “fingers”, “palm” and “thumb” domains. The structure of EV71 RdRp (3D^{pol})/GTP complex we reported here reveals the significant residues for ribonucleotide substrate binding, and captures a conformation of the polymerase to fit the substrate with two distinct movements

from the apoenzyme structure. The ribonucleotide analogue Br-UTP in the EV71 RdRp ($3D^{pol}$)/Br-UTP complex binds to the enzyme in a mode similar to that in the EV71 RdRp ($3D^{pol}$)/GTP complex, and trigs the similar conformational changes of the polymerase, pointing towards further structural based inhibitor design. Based on information derived from a model of the EV71 RdRp ($3D^{pol}$) in complex with the template:primer, the fingers domain is suggested to be involved in template binding, while the thumb domain should contribute to primer binding. The detailed structural information of EV71 RdRp ($3D^{pol}$) and its complex, in concert with previous studies of other polymerases, guides us to design inhibitors of EV71 RdRp ($3D^{pol}$) with good selectivity and potency.

All of these results establish EV71 RdRp ($3D^{pol}$) as a potential target for drug discovery. The structures reported here should provide a starting point for the development of therapeutics against EV71, which are urgently required in response to the pandemic of HFMD among Chinese children.

MATERIALS AND METHODS

Protein expression, purification and crystallization

The genomic region coding for the 3D polymerase of EV71 was amplified by PCR from the complete genome (EU131776) of human enterovirus 71 strain N3340-TW-02, adding a TEV protease cleavage site at the very upstream of the $3D^{pol}$ coding region using the primers 5'-CG**GGATCC**GAGAATCTTTATTTCCAGGGAGAGATC-CAGTGGGTTA-3' and 5'-CG**GAATTC**CTAAAATAACTCGAGCCAA-3', cloned into the pGEX-6p-1 vector (GE Healthcare) using BamH1 and EcoR1 restriction sites (shown in bold).

The recombinant plasmid was transformed into *Escherichia coli* strain BL21 (DE3). Ampicillin-resistant colonies were grown in LB medium at 37°C until the OD_{600} reached 0.6–0.8. Isopropyl β-D-1-thiogalactopyranoside (IPTG) was then added to a final concentration of 0.1 mM and the cultures grown for an additional 15–17 h at 16°C. Cells were harvested by centrifugation, resuspended and sonicated in the lysis buffer (20 mM Tris-HCl, pH 8.0, 500 mM NaCl, 1 mM DTT, 0.1 mM EDTA, 1 mM PMSF). The lysate was centrifuged at 20,000 g for 30 min to remove cell debris. The supernatant was loaded onto a glutathione sepharose column (GE Healthcare). After extensive washing with 20 mM Tris buffer pH 8.0, 500 mM NaCl, 1 mM DTT, the GST moiety was cleaved by His-tagged TEV protease in the same wash buffer at 4°C overnight. The protein was passed through a Ni^{2+}-NTA agarose column (Qiagen) to eliminate the His-tagged TEV protease, and then changed into a buffer containing 20 mM Tris, pH 8.0, 15% glycerol, 100 mM NaCl, 1 mM DTT by ultrafiltration. This was then loaded onto a Resource Q column and eluted with a linear gradient to 350 mM NaCl with 20 mM Tris pH 8.0, 15% glycerol, 1 mM DTT. Upon elution from the column, the protein was estimated to be > 99% pure from SDS-PAGE. The protein was concentrated to ~12 mg/mL in 20 mM Tris pH 8.0, 300 mM NaCl, 1 mM DTT. Protein concentrations were determined by absorbance at 280 nm using extinction coefficients obtained from the Expasy web site (http://www.expasy.org/tools/protparam.html).

Crystallization of EV71 RdRp ($3D^{pol}$) was performed at 18°C using the hanging-drop vapor-diffusion method. Crystals appeared and reached their final size in 4 d with a well solution containing 1.3 M ammonium sulfate, 0.1 M Bis-tris pH 6.1, 1 mM DTT and 10 mM $NiCl_2$. Crystals were soaked for 12 h at 18°C in a solution containing either 20 mM GTP (Sigma) or Br-UTP (Sigma) in the crystallization mixture listed above. All crystals were transferred into corresponding precipitant/ligand solutions containing 20% (*v/v*) glycerol prior to freezing and stored in liquid nitrogen for data collection.

X-day data collection, processing, and structure determination

The diffraction data were collected at 100 K using an ADSC Q270 detector on beamline BL17 of the Photon Factory (PF) in Japan. Data were processed and scaled using the HKL2000 package (Otwinowski and W., 1997).

The initial structure solution of EV71 RdRp ($3D^{pol}$) was obtained by molecular replacement using the program PHASER (McCoy et al., 2007) with the crystal structure of poliovirus polymerase (PDB code 1RA6) as a search model. The structure of the unliganded EV71 RdRp ($3D^{pol}$) was used as a starting model to obtain the structures of the EV71 RdRp ($3D^{pol}$) complex with GTP and Br-UTP, respectively. Manual model building and refinement were performed with COOT (Emsley and Cowtan, 2004) and CNS (Brunger et al., 1998) following rigid body refinement, energy minimization and individual B-factor refinement. Solvent molecules were located from stereochemically reasonable peaks in the σA-weighted $2F_o–F_c$ difference electron density map. The quality of the final refined model was verified using the program PROCHECK (Laskowski et al., 1993). Final refinement statistics are summarized in Table 1. Structural figures were drawn with the program PyMOL (DeLano, 2002).

ACKNOWLEDGMENTS

We thank Dr. Qi Jin from CDC for providing the EV71 genome. This work was supported by the National Basic Research Program (973 Program) and the National Programs for High Technology Research and Development Program (863 Program) (Grant Nos. 2006CB806503, 2006AA020502), National Major Project (Grant Nos. 2009ZX10004-304, 2009ZX09311-001), Tsinghua University Initiative Scientific Research Program (Grant No, 2009THZ01).

ABBREVIATIONS

Br-UTP, 5-bromouridine 5'-triphosphate; DdDps, DNA-dependent DNA polymerases; DMSO, Dimethyl sulfoxide; DTT, DL-Dithiothreitol; EV71, enterovirus 71; FMDV, foot-and-mouth disease virus; HFMD, hand-foot-and-mouth disease; IPTG, Isopropyl β-D-1-Thiogalactopyranoside; NTP, ribonucleoside triphosphate; RdRp, RNA-dependent RNA polymerase; rNTP, ribonucleotide; RT, reverse transcriptase

REFERENCES

Andino, R., Rieckhof, G.E., Achacoso, P.L., and Baltimore, D. (1993). Poliovirus RNA synthesis utilizes an RNP complex formed around the 5'-end of viral RNA. EMBO J 12, 3587–3598.

Bressanelli, S., Tomei, L., Roussel, A., Incitti, I., Vitale, R.L., Mathieu, M., De Francesco, R., and Rey, F.A. (1999). Crystal structure of the

RNA-dependent RNA polymerase of hepatitis C virus. Proc Natl Acad Sci U S A 96, 13034–13039.

Brunger, A.T., Adams, P.D., Clore, G.M., DeLano, W.L., Gros, P., Grosse-Kunstleve, R.W., Jiang, J.S., Kuszewski, J., Nilges, M., Pannu, N.S., *et al*. (1998). Crystallography & NMR system: a new software suite for macromolecular structure determination. Acta Crystallogr D Biol Crystallogr 54, 905–921.

Butcher, S.J., Grimes, J.M., Makeyev, E.V., Bamford, D.H., and Stuart, D.I. (2001). A mechanism for initiating RNA-dependent RNA polymerization. Nature 410, 235–240.

Campagnola, G., Weygandt, M., Scoggin, K., and Peersen, O. (2008). Crystal structure of coxsackievirus B3 $3D^{pol}$ highlights the functional importance of residue 5 in picornavirus polymerases. J Virol 82, 9458–9464.

Choi, K.H., Gallei, A., Becher, P., and Rossmann, M.G. (2006). The structure of bovine viral diarrhea virus RNA-dependent RNA polymerase and its amino-terminal domain. Structure 14, 1107–1113.

DeLano, W.L. (2002). The PyMOL Molecular Graphics System.

Domingo, E., Martin, V., Perales, C., and Escarmis, C. (2008). Coxsackieviruses and quasispecies theory: evolution of enteroviruses. Curr Top Microbiol Immunol 323, 3–32.

Doublie, S., Tabor, S., Long, A.M., Richardson, C.C., and Ellenberger, T. (1998). Crystal structure of a bacteriophage T7 DNA replication complex at 2.2 A resolution. Nature 391, 251–258.

Emsley, P., and Cowtan, K. (2004). Coot: model-building tools for molecular graphics. Acta Crystallogr D Biol Crystallogr 60, 2126–2132.

Ferrer-Orta, C., Agudo, R., Domingo, E., and Verdaguer, N. (2009). Structural insights into replication initiation and elongation processes by the FMDV RNA-dependent RNA polymerase. Curr Opin Struct Biol 19, 752–758.

Ferrer-Orta, C., Arias, A., Escarmis, C., and Verdaguer, N. (2006). A comparison of viral RNA-dependent RNA polymerases. Curr Opin Struct Biol 16, 27–34.

Ferrer-Orta, C., Arias, A., Perez-Luque, R., Escarmis, C., Domingo, E., and Verdaguer, N. (2004). Structure of foot-and-mouth disease virus RNA-dependent RNA polymerase and its complex with a template-primer RNA. J Biol Chem 279, 47212–47221.

Hansen, J.L., Long, A.M., and Schultz, S.C. (1997). Structure of the RNA-dependent RNA polymerase of poliovirus. Structure 5, 1109–1122.

Huang, H., Chopra, R., Verdine, G.L., and Harrison, S.C. (1998). Structure of a covalently trapped catalytic complex of HIV-1 reverse transcriptase: implications for drug resistance. Science 282, 1669–1675.

Jacobo-Molina, A., Ding, J., Nanni, R.G., Clark, A.D., Jr., Lu, X., Tantillo, C., Williams, R.L., Kamer, G., Ferris, A.L., Clark, P., *et al*. (1993). Crystal structure of human immunodeficiency virus type 1 reverse transcriptase complexed with double-stranded DNA at 3.0 Å resolution shows bent DNA. Proc Natl Acad Sci U S A 90, 6320–6324.

King, A.M.Q., Brown, F., Christian, P., Hovi, T., Hyypia, T. *et al*. (2000). Picornaviridae. In: Virus taxonomy. Seventh report of the international committee for the taxonomy of viruses (Van Regen-mortel, M.H.V., Fauquet, C.M., Bishop, D.H.L., Calisher, C.H. *et al*., Eds), pp. 657–673.

Laskowski, R., MacArthur, M., Moss, D., and Thornton, J. (1993). PROCHECK: a program to check the stereochemical quality of protein structures. J Appl Cryst 26, 283–291.

Lesburg, C.A., Cable, M.B., Ferrari, E., Hong, Z., Mannarino, A.F., and Weber, P.C. (1999). Crystal structure of the RNA-dependent RNA polymerase from hepatitis C virus reveals a fully encircled active site. Nat Struct Biol 6, 937–943.

Li, Y., Korolev, S., and Waksman, G. (1998). Crystal structures of open and closed forms of binary and ternary complexes of the large fragment of Thermus aquaticus DNA polymerase I: structural basis for nucleotide incorporation. EMBO J 17, 7514–7525.

Love, R.A., Maegley, K.A., Yu, X., Ferre, R.A., Lingardo, L.K., Diehl, W., Parge, H.E., Dragovich, P.S., and Fuhrman, S.A. (2004). The crystal structure of the RNA-dependent RNA polymerase from human rhinovirus: a dual function target for common cold antiviral therapy. Structure 12, 1533–1544.

Malet, H., Egloff, M.P., Selisko, B., Butcher, R.E., Wright, P.J., Roberts, M., Gruez, A., Sulzenbacher, G., Vonrhein, C., Bricogne, G., *et al*. (2007). Crystal structure of the RNA polymerase domain of the West Nile virus non-structural protein 5. J Biol Chem 282, 10678–10689.

Marcotte, L.L., Wass, A.B., Gohara, D.W., Pathak, H.B., Arnold, J.J., Filman, D.J., Cameron, C.E., and Hogle, J.M. (2007). Crystal structure of poliovirus 3CD protein: virally encoded protease and precursor to the RNA-dependent RNA polymerase. J Virol 81, 3583–3596.

Matthews, B.W. (1968). Solvent content of protein crystals. J Mol Biol 33, 491–497.

McCoy, A., Grosse-Kunstleve, R., Adams, P., Winn, M., Storoni, L., and Read, R. (2007). Phaser crystallographic software. J Appl Cryst 40, 658–674.

McMinn, P.C. (2002). An overview of the evolution of enterovirus 71 and its clinical and public health significance. FEMS Microbiol Rev 26, 91–107.

Ng, K.K., Arnold, J.J., and Cameron, C.E. (2008). Structure-function relationships among RNA-dependent RNA polymerases. Curr Top Microbiol Immunol 320, 137–156.

Ng, K.K., Cherney, M.M., Vazquez, A.L., Machin, A., Alonso, J.M., Parra, F., and James, M.N. (2002). Crystal structures of active and inactive conformations of a caliciviral RNA-dependent RNA polymerase. J Biol Chem 277, 1381–1387.

O'Reilly, E.K., and Kao, C.C. (1998). Analysis of RNA-dependent RNA polymerase structure and function as guided by known polymerase structures and computer predictions of secondary structure. Virology 252, 287–303.

Otwinowski, Z., and W., M. (1997). Processing of X-ray diffraction data collected in oscillation mode. Methods Enzymol 276, 307–326.

Poch, O., Sauvaget, I., Delarue, M., and Tordo, N. (1989). Identification of four conserved motifs among the RNA-dependent polymerase encoding elements. EMBO J 8, 3867–3874.

Racaniello, V.R. (2001). Picornaviridae: the viruses and their replication. In Fields Virology, DM Knipeand PM Howley, eds (Philadelphia: Lippincott Williams & Wilkins), pp. 685–722.

Salgado, P.S., Makeyev, E.V., Butcher, S.J., Bamford, D.H., Stuart, D. I., and Grimes, J.M. (2004). The structural basis for RNA specificity and Ca^{2+} inhibition of an RNA-dependent RNA polymerase. Structure 12, 307–316.

Tao, Y., Farsetta, D.L., Nibert, M.L., and Harrison, S.C. (2002). RNA

synthesis in a cage—structural studies of reovirus polymerase lambda3. Cell 111, 733–745.

Thompson, A.A., Albertini, R.A., and Peersen, O.B. (2007). Stabilization of poliovirus polymerase by NTP binding and fingers-thumb interactions. J Mol Biol 366, 1459–1474.

Thompson, A.A., and Peersen, O.B. (2004). Structural basis for proteolysis-dependent activation of the poliovirus RNA-dependent RNA polymerase. EMBO J 23, 3462–3471.

Yang, Y., Wang, H., Gong, E., Du, J., Zhao, X., McNutt, M.A., Wang, S., Zhong, Y., Gao, Z., and Zheng, J. (2009). Neuropathology in 2 cases of fatal enterovirus type 71 infection from a recent epidemic in the People's Republic of China: a histopathologic, immunohistochemical, and reverse transcription polymerase chain reaction study. Hum Pathol 40, 1288–1295.

Yap, T.L., Xu, T., Chen, Y.L., Malet, H., Egloff, M.P., Canard, B., Vasudevan, S.G., and Lescar, J. (2007). Crystal structure of the dengue virus RNA-dependent RNA polymerase catalytic domain at 1.85-angstrom resolution. J Virol 81, 4753–4765.

Zamyatkin, D.F., Parra, F., Alonso, J.M., Harki, D.A., Peterson, B.R., Grochulski, P., and Ng, K.K. (2008). Structural insights into mechanisms of catalysis and inhibition in Norwalk virus polymerase. J Biol Chem 283, 7705–7712.

